Supporting Information

High-Performance Graphene Sponges Reinforced with Polyimide for

Room Temperature Piezoresistive Sensing

Jingxia Huang [†,‡], Jinqing Wang *[,†], Zhigang Yang [†], and Shengrong Yang [†]

† State Key Laboratory of Solid Lubrication, Lanzhou Institute of Chemical Physics, Chinese Academy of Sciences, Lanzhou 730000, P. R. China.

‡ University of Chinese Academy of Sciences, Beijing 100049, P. R. China

* Corresponding author.

Tel: +86-931-4968076; Fax: +86-931-4968019.

E-mail address: jqwang@licp.cas.cn (J. Q. Wang)

S1 Reaction Schemes of Water-soluble Polyimide (PI) Precursor and Three-Dimensional Graphene (3DG) with the poly (amic Acid) ammonium Salt (PAS)
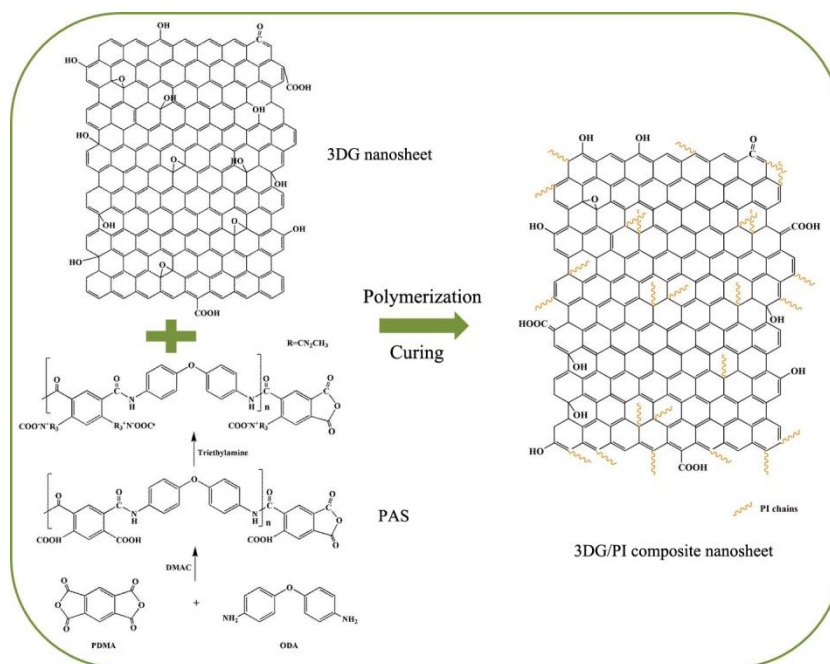

Figure S1 Reaction schemes of water-soluble PI precursor and polymerization scheme of 3DG with PAS.

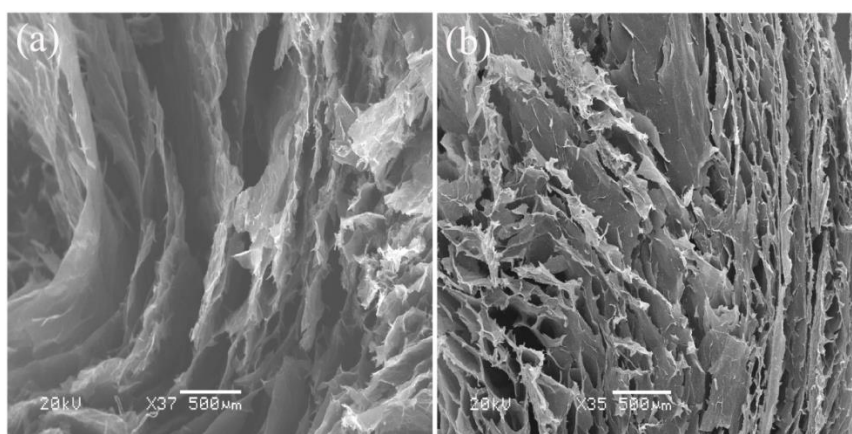## S2 Scanning Electron Microscope (SEM) Images of 3DG Sponge

Figure S2 SEM images of 3DG-10 sponge (a) and 3DG-10/PI composite sponge (b) with a porous interior like a bread.

S3 Transmission Electron Microscopy (TEM) Image of Graphene oxide (GO)

As shown in Figure S3, TEM image of GO nanosheets presents a typical 2D sheet-like morphology with some ripples on their surfaces, and the wrinkle structure ascribed to the point defects in the carbon lattice and sp^3 centers[1], which were generated by the severe oxidation process. In addition, the GO nanosheets with the average area and thickness of ~3.91 μm^2 and ~1.23 nm were clearly presented in atomic force microscopy (AFM) image (Figure S4).
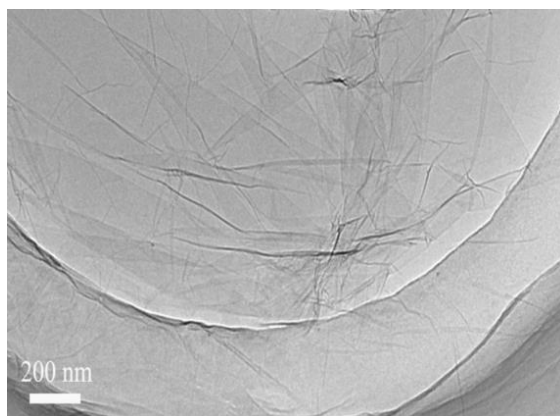

Figure S3 TEM image of GO nanosheets.

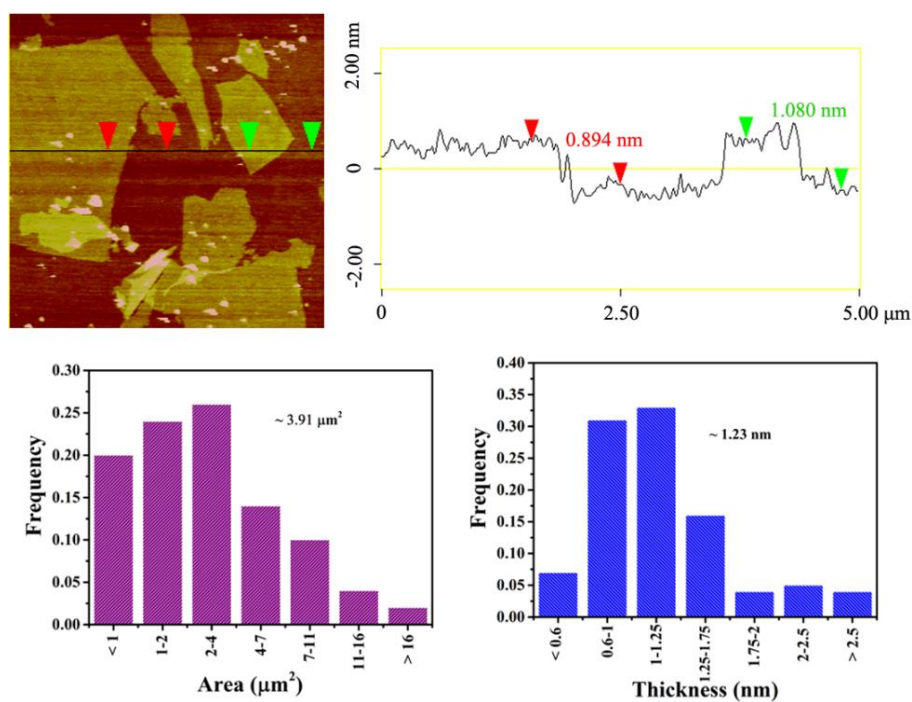**S4 AFM Characterization of GO Nanosheets**

Figure S4 AFM image and the corresponding height profile of GO nanosheets, as well as the area and thickness distributions of GO nanosheets.

S5 Physical Property of Graphene-based Composite Sponges

Table S1. Physical Properties of 3DG Sponge Prepared from the GO Solution with Different Initial Concentrations

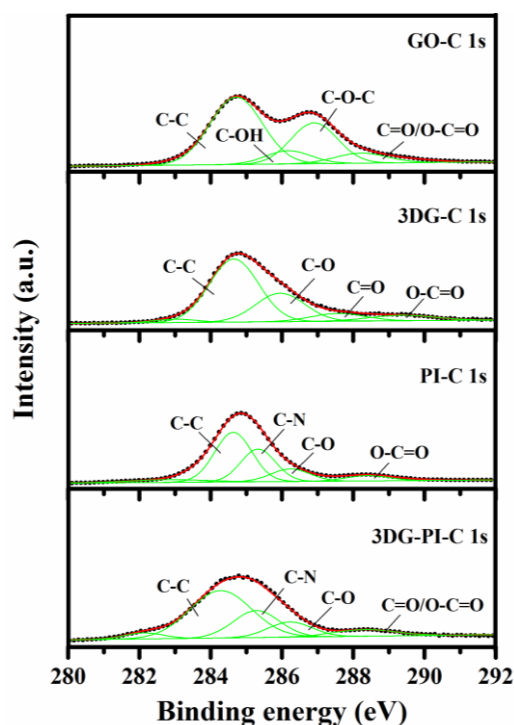| samples	GO concentration (mg/mL)	3DG bulk density ρ (mg/cm^3)	specific surface area (m^2/g)
3DG-3	3	9.4	200
3DG-5	5	14.3	218
3DG-7	7	16.9	214
3DG-10	10	20.2	142
3DG-15	15	22.7	134

S6 The XPS C 1s Spectra of Samples

Figure S5 C 1s fitted peaks in the XPS spectra of 3DG/PI composite sponge and contrast samples.

The C1s XPS spectra depicting the detailed surface composition of these samples were illustrated in Figure S5. As expected, regular peaks of oxygen-containing groups can be clearly observed from the C 1s spectrum of GO[2]. Besides, the dominant peak at 286.4 eV indicates the most oxygen-containing functional groups are epoxy groups. As for the C 1s spectrum of 3DG, the peak intensity of oxygen-containing functional groups decreases obviously, even disappearance, implying a high degree of reduction after solvothermal reaction. The C 1s spectrum of PI was fitted with four components, located at 284.4 eV, 285.6 eV, 286.3 eV and 288.6 eV, corresponding to the C=C/C–C, C–N, C–O–C/C–OH, and C=O groups[3], respectively. However, the characteristic C–N

peak could be seen at 285.6 eV for 3DG-5/PI composite sponge, indicating both components coexisted in the composite.

S7 X-ray Powder Diffraction (XRD) Patterns of Samples

Figure S6 shows the XRD patterns of 3DG and 3DG-5/PI composite sponges. For 3DG sponge, the broad XRD peak at 2θ=15-30 °C indicates the poor ordering of the graphene nanosheets along their stacking direction, and also reflects that the network of the sponge is composed of few-layer stacked graphene nanosheets.[1] In comparison, a shoulder peak at 2θ appears for 3DG after the thermal condensation, suggesting the composite was successfully obtained, implying that the PI possesses an upper degree of crystallinity, which is very different from that of amorphous PI prepared by a conventional solution process.[4-5] Herein, the crystallinity of PI ascribed to its typical melt-annealing synthetic process, because the thermal annealing can greatly affect the crystalline texture of a semiconducting polymer such as chain orientation and molecular ordering. Pyromellitic dianhydride (PMDA) molecules first reach a molten state and react with adjacent oxydianiline (ODA) molecules to form oligomeric polyimides. Subsequently, these oligomers crystallize from the monomer melt with the aid of hydrogen-bonding or π-π electronic interactions between the conjugated core units, resulting in upper symmetry and regularity of polymer chains.[6]
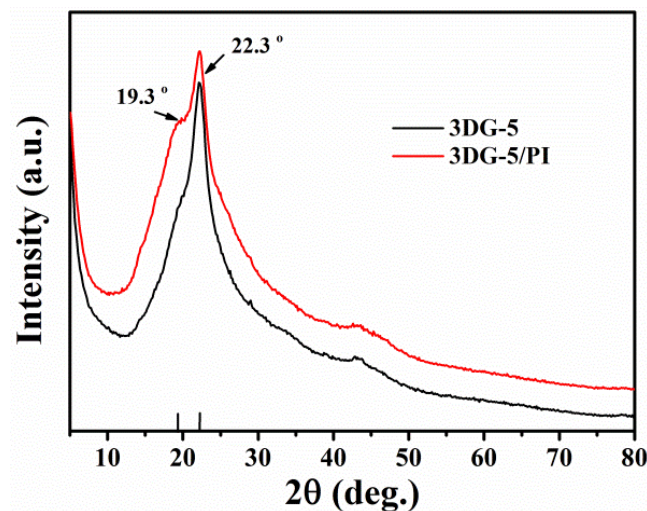
Figure S6 XRD patterns of 3DG scaffold and 3DG/PI composite sponge.

S8 Electrical Conductivity of 3DG Bulks and 3DG/PI Composite Sponges

The electrical conductivities of 3DG scaffolds and 3DG/PI composite sponges are shown in Figures S7a,b, where are compared with those of other 3DG bulks and graphene-based polymer composites reported in some literatures.
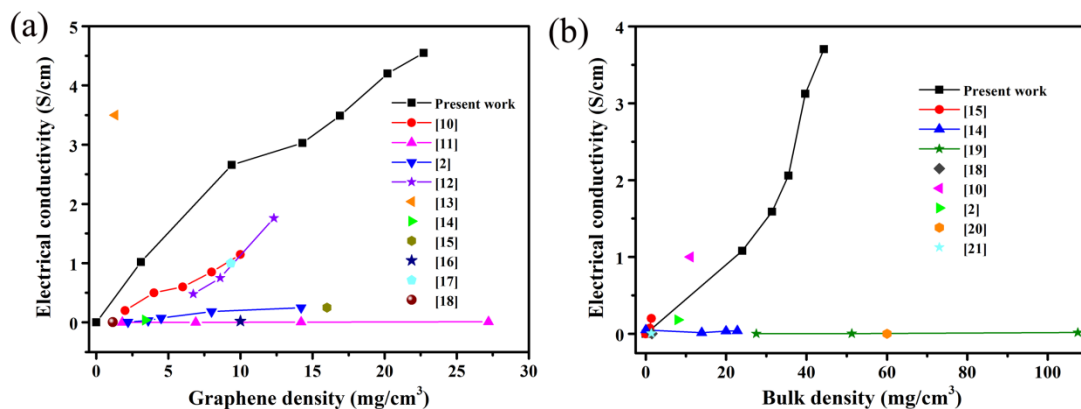

Figure S7 Electrical conductivities of 3DG bulks with graphene density (a) and 3DG/PI composite sponges with the bulk density (b), which were compared with the results reported in other works.

S9 Mechanical Performance of 3DG Sponges

The stress-strain (σ-ε) curves of the 3DG-15 sponges for the loading–unloading cycles at different set strains of 10%-50% and the cyclic stability at 50% strain were investigated. Apparently, the σ-ε curves for loading process contain three distinct deformation stages: the linear-elastic regime at $\varepsilon < 10\%$ with an elastic modulus just over about 19 kPa, which records the elastic bending of cell wall; plastic deformation stage at $10\% <\varepsilon< 45\%$ and an densification stage with a steep rise in stress at $\varepsilon > 45\%$, as shown in Figure S8a. Moreover, the energy loss coefficient (ξ) and Young's modulus (E) respectively reduced by 19.4% and 16.5% during the repeated compression; meanwhile, the ultimate stress (σ_u) at 50% strain shows slight degradation from 14.7 kPa to 12.6 kPa, as calculated in the inset of the Figure S8b. However, the total loss strain (η) increased by 3% (see Figure S8c), reflecting the eminent resilient property of 3DG sponge, attributing to the most recover of thickness for graphene cylinder after the external load was removed during the repeated compression.[7] Again, the compressive property of 3DG-15 at different strain rates of 10%-1000%/min were also presented in Figure S8d, where the σ-ε curves almost overlap each other and each succeeding loading curve almost can return to the maximum stress point, suggesting perfect strain memory effects, ascribing to the well-networked structure, elasticity and flexibility of 3DG sponge. Also, the ξ exhibits a tiny decrease from 49% to 46.5%, due to the friction or fracture during deformation and the unbinding of the walls during the unloading process.[8] Compressive schematic and snapshots during the compressive testing are shown in Figure S8e.
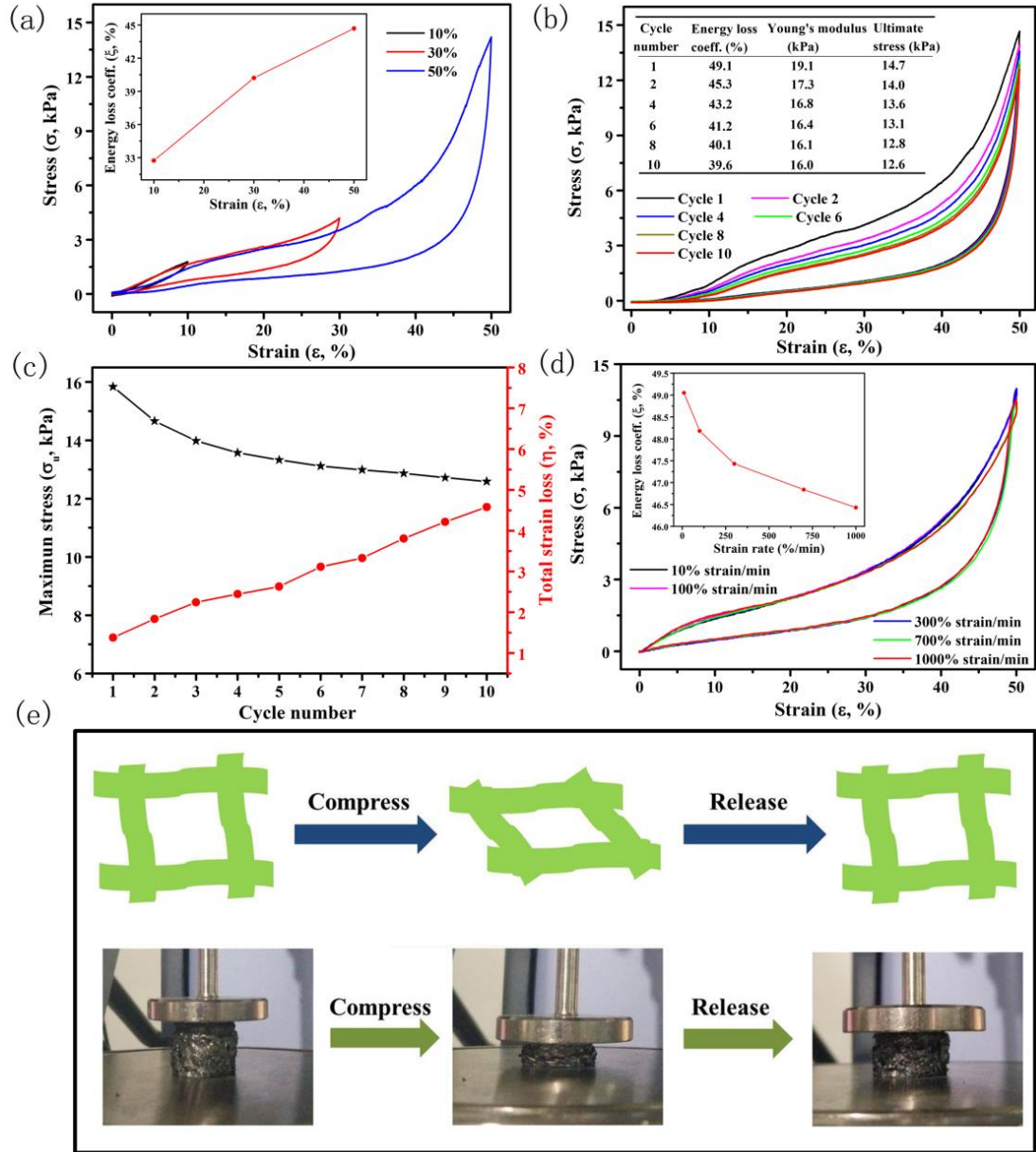
The table in panel (b):

Cycle number	Energy loss coeff. (%)	Young's modulus (kPa)	Ultimate stress (kPa)
1	49.1	19.1	14.7
2	45.3	17.3	14.0
4	43.2	16.8	13.6
6	41.2	16.4	13.1
8	40.1	16.1	12.8
10	39.6	16.0	12.6

Figure S8 Mechanical properties of 3DG-15 sponge: (a) Compressive σ-ε curves at different strains; the inset shows the ξ curve with strain. (b) Mechanical stability after 10 loading–unloading cycles under a compressive strain of 50%. The inset lists the calculated values of ξ, E and σ_u. (c) Retention of maximum stress at a strain of 50% and η during 10 cycles. (d) Compressive σ-ε curves under a strain of 50% at different set strain rates. The inset shows the ξ curve with the strain rate. (e) The compressive schematic and snapshots during the compressive testing.
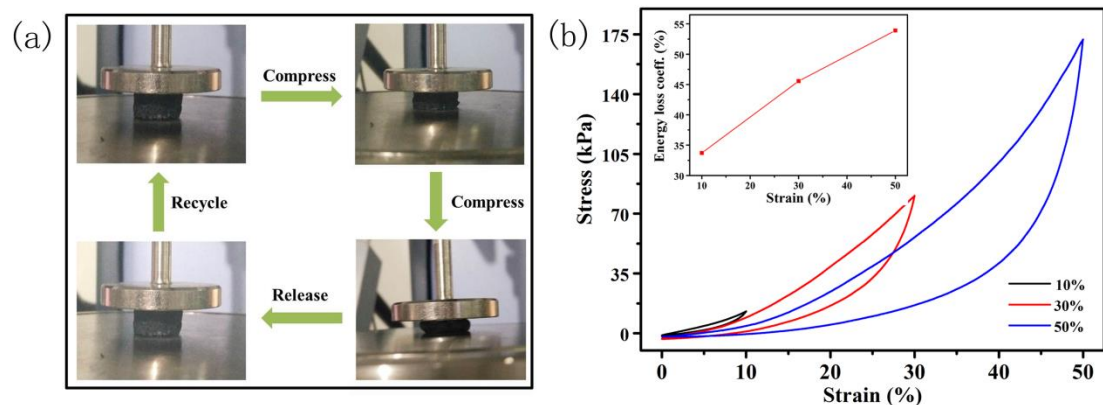
S10 PI and 3DG-5/PI Composite Sponges

Figure S9 (a) Snapshots in the compressive testing of 3DG-5/PI composite sponge; (b) the compressive σ-ε curves of PI monolith at different strains of 10%, 30%, and 50%. The inset shows the varation of ξ with the strain.

S11 Electromechanical Performance of 3DG-15 Monolith

As presented in Figure S10a, the current-voltage (*I*-*V*) curves of 3DG-15 sponges at different compressive strains of 0%-60% exhibited the good linear characteristics, and the slope of *I*-*V* curves increases with the rising strain. Moreover, the resistance response to compression cycles of 10 is also given in Figure S10b; apparently, when compression strain increased from 15% to 60%, the change of resistance variation ratio ((R_0-R)/R_0), where R and R_0 represent the resistance with and without strain, increased from about 20% to 54%. The super electromechanical performance is attributed to the porous and lamellar structures of sponge compressed gradually, which generated the wrinkling and buckling cell walls and increased the contact areas of graphene nanosheets in 3DG monolith, thusly building up the conductive pathways for electron transport. Once the external stress is moved, the sponge can be recovered

almost completely, and its conductive networks can recover the original state to obtain the almost unchanged electrical resistance.[9]
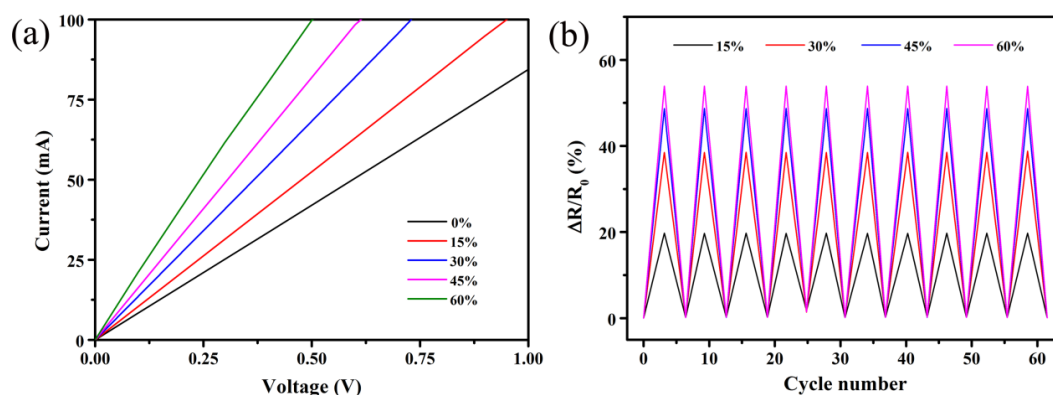

Figure S10 (a) *I-V* curves and (b) resistance variation ratio of 3DG-15 composite sponges under different compressive strains for 10 cycles.

REFERENCES

(1) Gómez-Navarro C.; Weitz R.; Bittner A.;Scolari.; Mews A.; Burghard M.; Kern K. Electronic Transport Properties of Individual Chemically Reduced Graphene Oxide Sheets. *Nano Lett.* **2007**, *7*, 3499-3503.

(2) Zhang, L. B.; Chen, G. Y.; Hedhili, M. N.; Zhang, H. N.; Wang, P. Three-Dimensional Assemblies of Graphene Prepared by A Novel Chemical Reduction-Induced Self-Assembly Method. *Nanoscale* **2012,** *4*, 7038-7045.

(3) Xu X.; Li H.; Zhang Q. Q.; Hu H.; Zhao Z. B.; Li J. H.; Li J. Y.; Qiao Y.; Gogotsi Y. Self-Sensing, Ultralight, and Conductive 3D Graphene/Iron Oxide Aerogel Elastomer Deformable in A Magnetic Field. *ACS Nano* **2015**, *9*, 3969-3977.

(4) Lee, T.; Park, S. S.; Jung, Y.; Han, S.; Han, D.; Kim, I.; Ha, C. S. Preparation and Characterization of Polyimide/Mesoporous Silica Hybrid Nanocomposites Based

on Water-Soluble Poly(amic acid) Ammonium Salt. *Eur. Polym. J.* **2009,** *45*, 19-29.

(5) Zhu, B. K.; Xie, S. H.; Xu, Z. K.; Xu, Y. Y. Preparation and Properties of the Polyimide/Multi-Walled Carbon Nanotubes (MWNTs) Nanocomposites. *Compos. Sci. Technol.* **2006,** *66*, 548-554.

(6) Chu, S.; Wang, Y.; Guo, Y.; Zhou, P.; Yu, H.; Luo, L. L.; Kong, F.; Zou, Z. G. Facile Green Synthesis of Crystalline Polyimide Photocatalyst for Hydrogen Generation from Water. *J. Mater. Chem.* **2012,** *22*, 15519-15521.

(7) Qiu, L.; Liu, J. Z.; Chang, S. L.; Wu, Y.; Li, D. Biomimetic Superelastic Graphene-Based Cellular Monoliths. *Nat. Commun.* **2012,** *3*, 1241.

(8) Barg, S.; Perez, F. M.; Ni, N.; do Vale Pereira, P.; Maher, R. C.; Garcia-Tuñon, E.; Eslava, S.; Agnoli, S.; Mattevi, C.; Saiz, E. Mesoscale Assembly of Chemically Modified Graphene into Complex Cellular Networks. *Nat. Commun.* **2014**, 5,4328.

(9) Guan, L. Z.; Gao, J. F.; Pei, Y. B.; Zhao, L.; Gong, L. X.; Wan, Y. J.; Zhou, H.; Zheng, N.; Du, X. S.; Wu, L. B.; Jiang, J. X.; Liu, H. Y.; Tang, L. C.; Mai, Y. W. Silane Bonded Graphene Aerogels with Tunable Functionality and Reversible Compressibility. *Carbon* **2016,** *107*, 573-582.

(10) Zhang, Q. Q.; Xu, X.; Li, H.; Xiong, G. P.; Hu, H.; Fisher, T. S. Mechanically Robust Honeycomb Graphene Aerogel Multifunctional Polymer Composites. *Carbon* **2015,** *93*, 659-670.

(11) Tang, G. Q.; Jiang, Z. G.; Li, X. F.; Zhang, H. B.; Dasari, A.; Yu, Z. Z. Three

Dimensional Graphene Aerogels and Their Electrically Conductive Composites. *Carbon* **2014,** *77*, 592-599.

(12) Li, Y. R.; Chen, J.; Huang, L.; Li, C.; Hong, J. D.; Shi, G. Q. Highly Compressible Macroporous Graphene Monoliths via An Improved Hydrothermal Process. *Adv. Mater.* **2014,** *26*, 4789-4793.

(13) Jia, J. J.; Sun, X. Y.; Lin, X. Y.; Shen, X.; Mai, Y. W.; Kim, J. K. Exceptional Electrical Conductivity and Fracture Resistance of 3D Interconnected Graphene Foam-Epoxy Composites. *ACS Nano* **2014**, *8*, 5774-5783.

(14) Lu, H.; Li, C. W.; Zhang, B. Q.; Qiao, X.; Liu, C. Y. Toward Highly Compressible Graphene Aerogels of Enhanced Mechanical Performance with Polymer. *RSC Adv.* **2016,** *6*, 43007-43015.

(15) Wang, Z. Y.; Shen, X.; Akbari Garakani, M.; Lin, X. Y.; Wu, Y.; Liu, X.; Sun, X. Y.; Kim, J. K. Graphene Aerogel/Epoxy Composites with Exceptional Anisotropic Structure and Properties. *ACS Appl. Mater. Inter.* **2015,** *7*, 5538-5549.

(16) Qin, Y. Y.; Peng, Q. Y.; Ding, Y. J.; Lin, Z. S.; Wang, C. H.; Li, Y. Lightweight, Superelastic, and Mechanically Flexible Graphene/Polyimide Nanocomposite Foam for Strain Sensor Application. *ACS Nano* **2015**, 9, 8933-8941.

(17) Peng, Q. Y.; Li, Y. B.; He, X. D.; Gui, X. C.; Shang, Y. Y.; Wang, C. H.; Wang, C.; Zhao, W. Q.; Du, S. Y.; Shi, E. X.; Li, P. X.; Wu, D. H.; Cao, A. Y. Graphene Nanoribbon Aerogels Unzipped from Carbon Nanotube Sponges. *Adv.*

Mater. **2014,** *26*, 3241-3247.

(18) Wu, C.; Huang, X. Y.; Wu, X. F.; Qian, R.; Jiang, P. K. Mechanically Flexible and Multifunctional Polymer-Based Graphene Foams for Elastic Conductors and Oil-Water Separators. *Adv. Mater.* **2013,** *25*, 5658-5662.

(19) Li, Y. Q.; Samad, Y. A.; Polychronopoulou, K.; Alhassan, S. M.; Liao, K. Highly Electrically Conductive Nanocomposites Based on Polymerinfused Graphene Sponges. *Sci. Rep.* **2014,** *4*, 4652.

(20) Huang, H.; Chen, P. W.; Zhang, X. T.; Lu, Y.; Zhan, W. C. Edge-to-Edge Assembled Graphene Oxide Aerogels with Outstanding Mechanical Performance and Superhigh Chemical Activity. *Small* **2013,** *9*, 1397-1404.

(21) Sun, H. Y.; Xu, Z.; Gao, C. Multifunctional, Ultra-Flyweight, Synergistically Assembled Carbon Aerogels. *Adv. Mater.* **2013,** *25*, 2554-2560.